Forebody and Inlet Design for the HIFiRE 2 Flight Test

Paul G. Ferlemann

ATK
Hampton, Virginia

JANNAF Airbreathing Propulsion Subcommittee Meeting
Boston, Massachusetts

May 12–16, 2008

Forebody and Inlet Design for the HIFiRE 2 Flight Test*

Paul G. Ferlemann
ATK
Hampton, Virginia

ABSTRACT

A forebody and inlet have been designed for the HIFiRE 2 scramjet flight test. The test will explore the operating, performance, and stability characteristics of a simple hydrocarbon-fueled scramjet combustor as it transitions from dual-mode to scramjet-mode operation and during supersonic combustion at Mach 8+ flight conditions. Requirements for the compression system were derived from inlet starting and combustor inflow requirements as well as physical size constraints. The design process is described. A planar, fixed geometry, mixed compression concept was used to produce laterally uniform flow at the inlet entrance and a conservative amount of internal contraction with respect to inlet starting. A grid sensitivity study was performed so that important flow physics caused by three-dimensional shock boundary layer interactions could be captured with confidence. Results from low Mach number operability studies, nominal trajectory cases, and high dynamic pressure heat load cases are discussed. The forebody and inlet solutions provide information for on-going combustor calculations, mass capture across the trajectory for fuel system design, and surface heating rates for thermal/structural analysis. The design has a one freestream Mach number margin for inlet starting, exceeds the high Mach number combustor entrance pressure requirement, produces high quality flow at the inlet exit for all Mach numbers and vehicle attitudes in the design space, and fits inside the booster shroud.

INTRODUCTION

Figure 1. HyShot 2 flight experiment.

The Hypersonic International Flight Research and Experimentation (HIFiRE) Program is a collaborative international effort to perform hypersonic research through flight experimentation.[1] The partners are Australia's Defense Scientific and Technology Office (DSTO) and the US Air Force Research Lab (AFRL). For the second flight in this program a two stage launch vehicle concept, similar to the HyShot[2] launch vehicle shown in Figure 1, is envisioned for delivering the experiment payload through the desired flight conditions. The HIFiRE 2 flight will employ a suppressed trajectory and perform the scramjet combustor test during the accelerating portion of the second stage burn. System requirements were derived based on the experiment window shown in Figure 2. The experiment window was defined based on preliminary trajectory studies which showed that a fairly constant dynamic pressure was achievable. The analysis indicated that 7 to 9 seconds were available for the scramjet test as the booster accelerated from Mach 5.5 to 8.5. The combustor will operate on a gaseous mixture of ethylene and methane as a surrogate fuel[3] for the thermally stressed JP-7 which would exist at the exit of a heat exchanger for a JP-7 cooled and fueled scramjet engine. Successful launch and operation will produce a valuable scramjet combustor data set and establish a new test capability to explore high enthalpy scramjet research and technologies.

---

* Approved for public release; distribution is unlimited.

* This work was supported by contract NNL07AA00B with the NASA Langley Research Center.

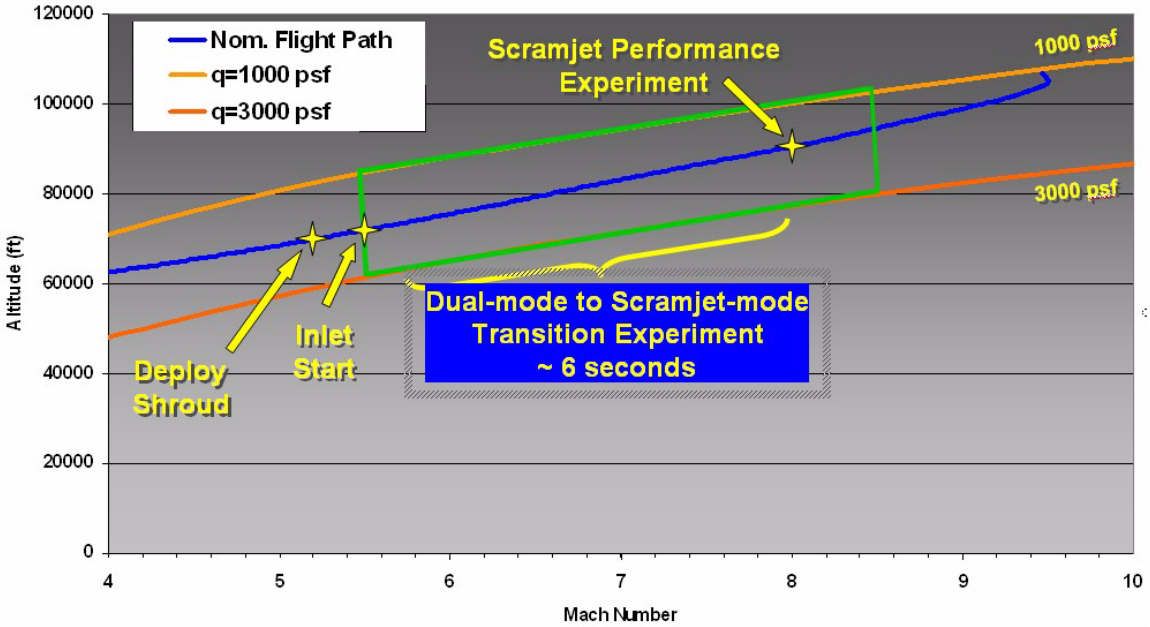

Figure 2. HIFiRE 2 nominal flight path and experiment window.

FOREBODY AND INLET DESIGN

REQUIREMENTS, CONSTRAINTS AND APPROACH

The primary objectives of the flight experiment are related to the hydrocarbon fueled scramjet combustor operation and performance. With the focus on combustor operation, it was desirable to minimize risk in all other areas of the experiment and system design. Therefore, a planar design solution was imposed so that two-dimensional shock boundary layer separation correlations were applicable. The forebody and inlet had to fit inside a 22 inch outer diameter nose cone shroud and interface with the pre-defined 1x4 inch isolator entrance. Ground testing for combustor development had used a 1.5x4 inch entrance dimension. The throat height was reduced to 1 inch for the flight experiment based on initial studies of required over-all contraction and payload size. The inlet had to start (establish supersonic flow) prior to Mach 5.5. The Kantrowitz criteria[4] for establishing supersonic flow in a fixed geometry inlet was selected as the design constraint for inlet starting. This criteria was applied at the inlet entrance using the one-dimensional flow Mach number. A one-dimensionalized static pressure of 1/2 atmosphere (7.35 psi) was required at the combustor entrance (which includes the pressure rise through an 8 inch long constant area isolator) at Mach 8.5 and 1000 psf dynamic pressure over a range of ±2° angle of attack based on combustor stability limits. Finally, a minimal boundary layer separation constraint was imposed at Mach 5.5 over ±2° angle of attack and ±2° angle of sideslip. This requirement allowed greater confidence in the flow calculations compared to flows with large scale separated regions and contributed to the research objective of designing and verifying by CFD, potentially with sufficient confidence to avoid an inlet ground test program.

Several desired features also influenced the design approach. Fixed geometry was highly desirable in order to reduce operational complexity, and the associated analysis, design, and manufacturing costs. The design was not a predecessor to any free-flying vehicle, therefore drag was not a major concern. This allowed considerable flexibility in the forebody design. Ultimately, this flexibility was used to maintain well behaved boundary layer flow. Well behaved boundary layer flow was desired, particularly at the inlet exit, so that the isolator would have the desired back-pressure capability and predictive models of isolator performance could be applied. Therefore, “well behaved” refers to the

minimization of boundary layer roll-up, streamwise vortices, or other local phenomena that could adversely affect isolator back-pressure capability. Although somewhat qualitative, it is assessed and discussed further in the results section. Minimizing the sensitivity of inlet mass capture and combustor entrance flow properties to booster dynamics was desired. Booster dynamics are likely to include some nutation and angle of attack variation. In addition, since a spin-stabilized flight is currently planned, even a constant angle of attack for the booster will result in a $+\alpha/+\beta/-\alpha/-\beta$ cyclical oscillation for the experiment. Therefore, a forebody and inlet design which is insensitive to α and β variations will contribute to achieving the intended fuel equivalence ratio schedule, stable combustor operation, and simplify post-flight data analysis. Finally, there was no "on design" flight Mach number.

INITIAL CONCEPTS

Imposing the use of 2D concepts to design the compression system limited the potential designs to be planar in the spanwise direction and to turn the flow in either an outward or inward direction, as shown in Figure 3. To limit the forebody (and shroud) length, a single compression angle from the nose was selected. The outward turning concept could use a shock trap (flow exhausted laterally), as shown for the top flowpath, or the cowl shock could be designed to cancel at the body shoulder for an on-design Mach number, as shown for the bottom flowpath. Significant challenges for the outward turning option were maintaining the desired flowpath scale while achieving sufficient overall contraction to meet the combustor entrance pressure requirement at Mach 8.5, maintaining a small amount of internal contraction, and the mass capture sensitivity to angle of attack. For these reasons, effort was focused on the inward turning option. The inward turning concept solved the flowpath scale and angle of attack sensitivity problems, but at the cost of a longer shroud, a sizable cantilevered forebody structure, and an increased nozzle length requirement to route the combustor exhaust overboard.

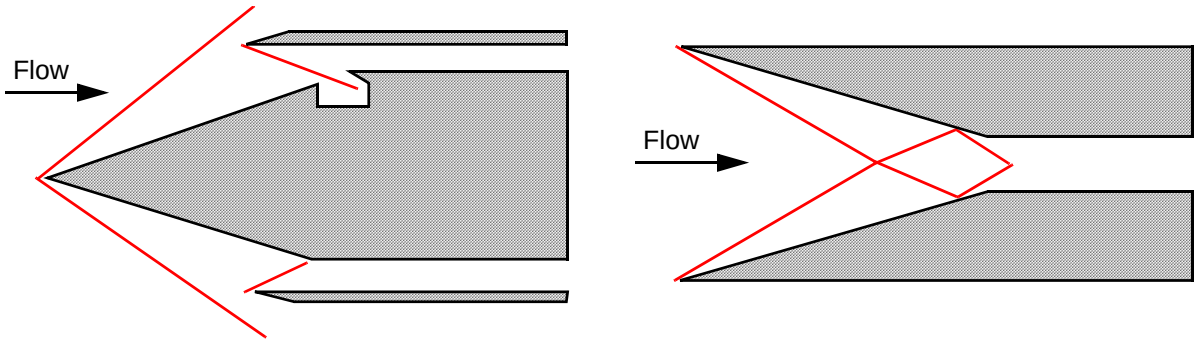

Figure 3. Single compression angle outward and inward turning concepts.

Two preliminary concepts are shown in Figure 4. The first, on the left, maintained the 4 inch isolator width projected forward to the forebody nose. An attempt to limit lateral spillage resulted in flow fences originating at the nose, which required a significant notch to limit the internal contraction. A second concept, shown at the right, investigated the effectiveness of widening the forebody to reduce lateral spillage. This image shows two flowpaths in a side-by-side orientation. The objectives of this concept were to maximize the external contraction and use the maximum width allowable at the end of the forebody to limit lateral spillage. Since drag was not a major concern, it was acceptable that the forebody compressed significantly more air than the inlet captured. This created an aerodynamic flow fence which laterally contained the captured air flow and produced a well behaved laterally uniform boundary layer at the inlet entrance. Based on encouraging results for the wider forebody design, this concept was selected for additional refinement. The design concept requires a forebody wide enough to create and maintain the aerodynamic flow fence affect to the inlet entrance. Three-dimensional computational methods were required during the conceptual design phase due to the sensitivity to lateral spillage.

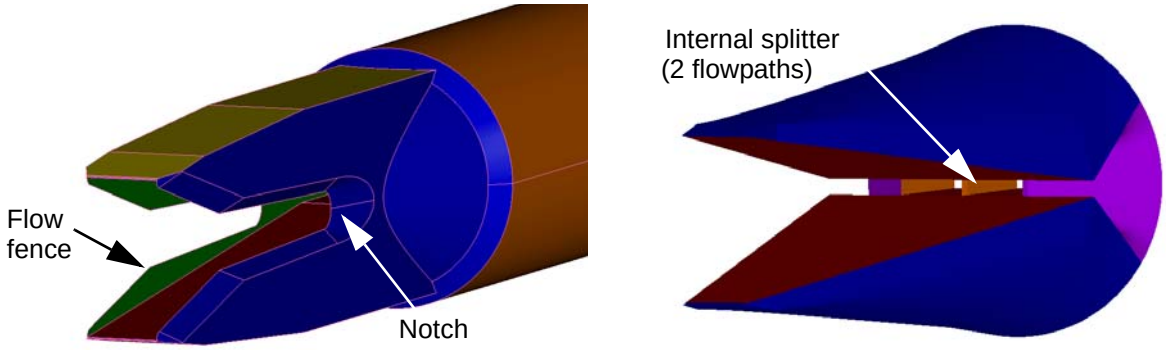

Figure 4. Constant and increasing width forebody concepts.

Capture Height, Forebody Width, and Internal Contraction Ratio Trade-offs

The configuration used to define the forebody geometric design space is shown in the left image of Figure 5. One quarter of the complete geometry is shown shaded. A single isolator/combustor flowpath was selected for refinement in order to reduce operational complexity and increase instrumentation density. The blue surface represents the forebody surface. The orange surface is an 18 inch diameter cylinder which defined the assumed maximum allowable working diameter corresponding to a 22 inch outer diameter shroud. The cylindrical portion of the shroud limits the forebody size, so the intersection of the blue and orange surfaces defined the maximum size forebody design space. The maximum size forebody (maximum air capture) was of interest since the Mach 8.5 combustor entrance pressure requirement (1/2 atm.) defined the required overall contraction (compression), but the Mach 5.5 inlet starting requirement limited the amount of allowable internal contraction. Therefore, the initial forebody design study investigated whether all of the contraction could be achieved externally, thereby producing the greatest possible margin for inlet starting (no internal contraction). As a result, there was no inlet and the isolator began at the end of the forebody. However, the maximum size forebody which could fit within the shroud was not a unique configuration since a range of geometries were possible depending upon where the forebody started along the intersection of the two surfaces. A longer forebody (increasing capture height) forces the nose to be narrower. Increased capture height results in greater initial mass capture, but a narrower nose results in increased lateral spillage. As a result, 3D computational tools were required to evaluate this trade-off. The images on the right side of Figure 5 show a sample design with the maximum allowable capture height.

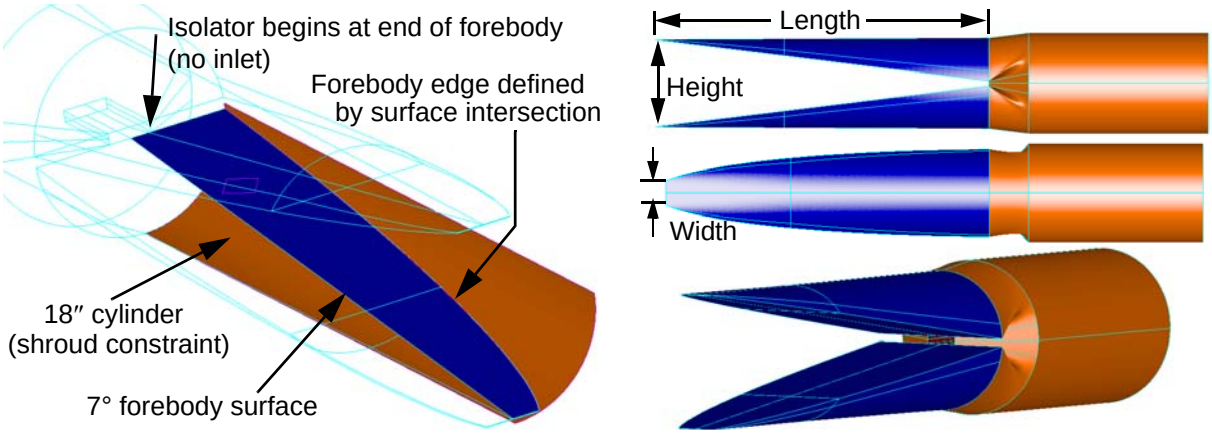

Figure 5. Initial forebody design space and sample design.

CFD solutions were performed for a range of forebody sizes. The computational approach is described after the grid convergence section of this paper. Throat pressure results plotted as a function of the capture-height versus leading-edge-width design space are shown on the left side of Figure 6. Four configurations were evaluated along the 18 inch inner working diameter curve. Results for two smaller configurations (from the conceptual design phase) are also included with a capture height of 11.7 inches and nose widths of 4 and 5 inches. Results from all cases were used to create the colored contour lines of throat pressure. The 1/2 atmosphere pressure requirement line is indicated. Therefore, a design with no internal contraction was possible, but would require a large forebody and shroud. In order to reduce the size of both components, the effectiveness of adding internal contraction was investigated. The Kantrowitz internal contraction ratio criteria for inlet starting[4] was used to calculate the allowable internal contraction based on the flux-conservative one-dimensional flow Mach number at the inlet entrance for the Mach 5.5 freestream condition. A value of 1.4 was calculated for the maximum internal contraction ratio but a value of 1.2 was selected to provide additional margin (corresponding to flight at Mach 4.5). The right side of Figure 6 shows two ways to add internal contraction. In the top image the inlet sidewall was moved forward on the forebody surface. Due to the width of the flowpath and the forebody compression angle, only a small distance was possible before the internal contraction ratio limit was reached. The bottom image shows a second alternative where the inlet sidewall leading edge has been moved outboard. An angle of 3° was selected for the sidewall compression angle based on design experience. The primary concern was limiting the strength of the shock sweeping across the forebody boundary layer. Significantly more air was captured with this option for a given amount of internal contraction. The effectiveness of adding internal contraction meant that the external contraction could be reduced. The result was a smaller forebody as indicated by the red symbol in the left image of Figure 6. Finally, when bluntness was added to the inlet sidewall leading edge, the throat pressure increased by 0.8 psi. A leading edge radius of 0.030 inches was selected for the forebody nose and inlet sidewall leading edges based on considerable experience[5] and leading edge thermal analysis A leading edge of this size produces acceptable blunt leading edge aerodynamic effects, is able to survive high local heating for short duration, and is large enough to allow an active cooling channel near the leading edge when necessary. The final material selection and detailed structural design are still in progress. Therefore, a design with a 12 inch capture height, 5 inch wide nose, and an internal contraction ratio of 1.2 met the Mach 5.5 internal contraction ratio and the Mach 8.5 combustor entrance pressure requirements with considerable margin.

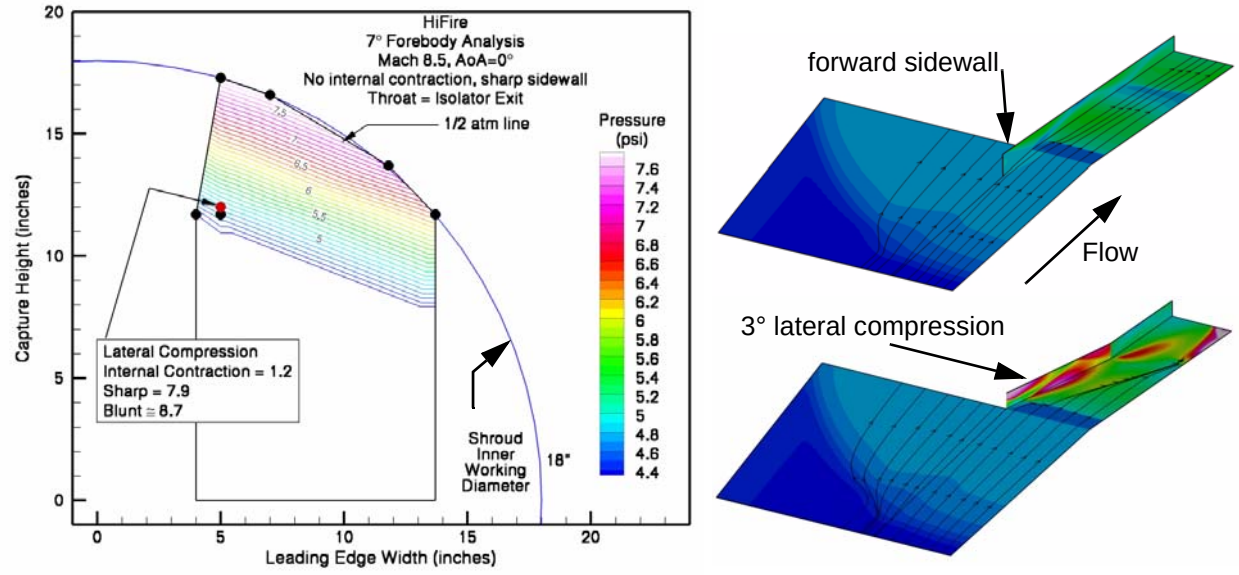

Figure 6. Throat pressure map for design space and internal contraction ratio concepts.

With the capture height and nose width defined, final sculpting of the forebody was performed. The final geometry and surface definitions are shown in Figure 7. The first step was to take advantage of the reduced capture height (relative to the maximum allowable capture height). This allowed the forebody to fit within the converging portion of a shroud, instead of only the cylindrical section. A surface approximating a 3:1 ogive (minimum aerodynamic drag nose cone shroud shape) was created and the intersection with the forebody surface redefined the outer edge of the forebody. An angle of 7° was selected for the forebody compression angle based on 2D shock/turbulent boundary layer separation criteria. Preliminary laminar calculations and a natural transition criteria based on the ratio of Reynolds number based on momentum thickness over the Mach number at the boundary layer edge (Re_θ/M_e=305) indicated that the forebody flow may not naturally transition to turbulent flow before the first shock reflection caused by the bow shock from the opposing side of the forebody. As a result, a boundary layer trip strip will be placed 15 inches from the nose, as shown in Figure 7. A trip design based on boundary layer thickness and the X-43A design process is envisioned.[6] The second step was to add a chine surface at the end of the forebody. The Mach wave angle (evaluated at the local flow Mach number from a Mach 5 flight solution) was used to define the forward edge of this surface. The purpose of the chine was to end the outboard forebody compression as soon as possible without affecting the captured flow. Relieving the flow pressure at the end of the forebody will facilitate spilling of flow not captured by the inlet, help inlet starting, and prevent any disturbance from the inlet external sidewall from affecting the captured flow. Figure 7 also includes a sectioned view of a conceptual payload design showing the experimental flowpath integration with a shroud and airframe structure.

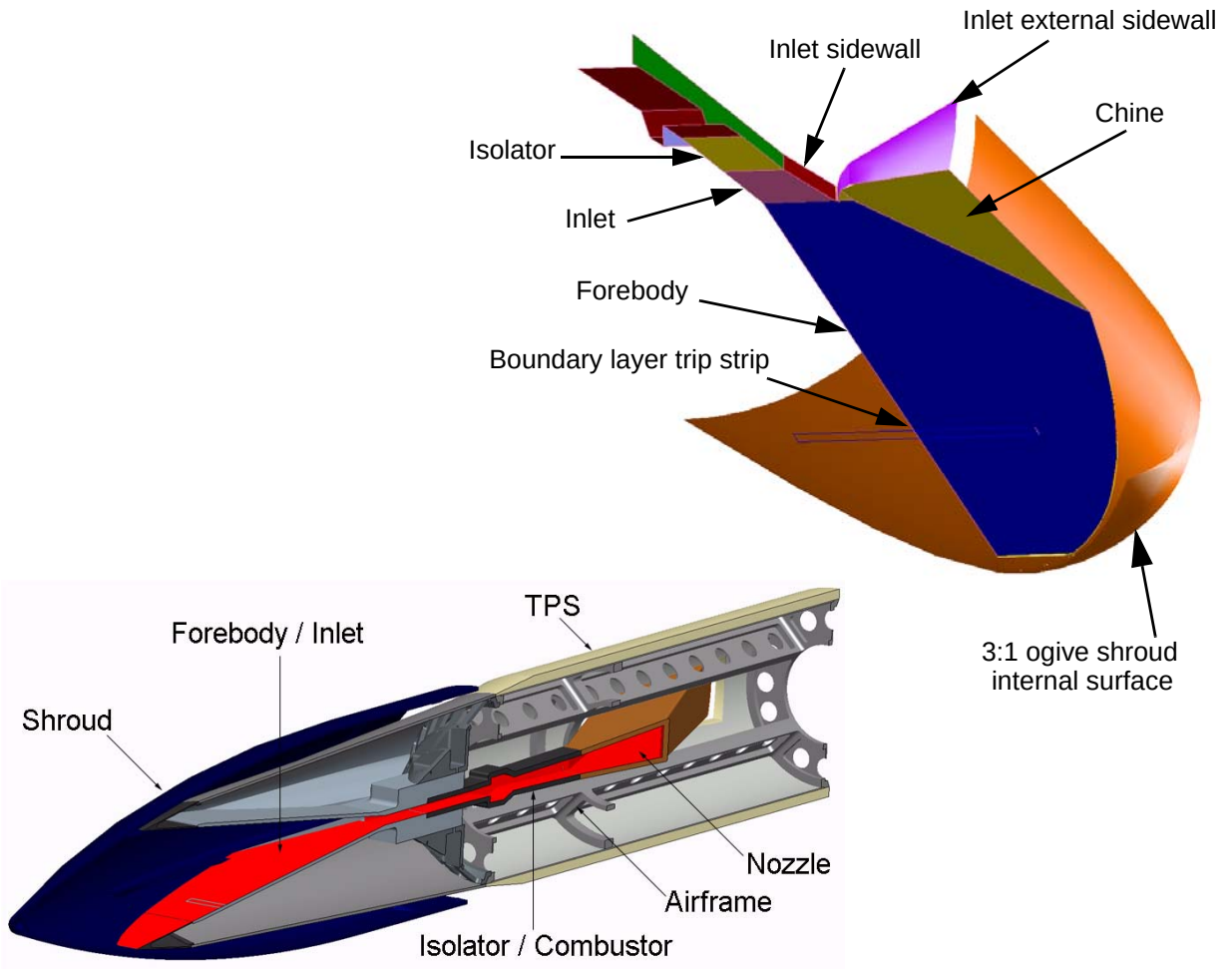

Figure 7. Forebody and inlet surface definitions (1/4 of full geometry shown) and sectioned view (1/2 of payload shown).

FINAL DESIGN FEATURES

A view from the nose looking aft and a perspective view are shown in Figure 8. Each of the following three figures shows surface pressure contours from an unfueled Mach 8 solution. The forebody leading edges are ±6 inches from the horizontal centerline and have a 0.030 inch radius with a 15° included angle. The total width for the cylindrical portion of the nose is 4.5 inches. The forebody surface angle is 7°. The leading edge of the nozzle centerbody is visible through the center of the engine. A view from the side of the payload is shown in Figure 9. The chine surface begins 30 inches from the nose. The chine outboard edge is at a constant vertical height, thereby ending compression at the end of the forebody outboard of a Mach line traced from a Mach 5 calculation. The forebody is 44.79 inches long and ends at a 1 inch flow height. The diameter at the end of the chine is 19.5 inches. The surface leading to the full 22 inch diameter is not final and will have to accommodate shroud attachment hardware. A planform view of the internal flowpath surfaces is included in Figure 10. The inlet sidewall leading edges have a 0.030 inch radius and a 15° included angle. The inlet produces lateral compression from a capture width of 4.8 inches to an isolator width of 4 inches over a distance of 7.63 inches (3° compression each sidewall). An 8 inch long constant area isolator leads to the combustor entrance. Flame holding cavities are used on each side of the combustor. Although included in the figures for perspective, the combustor[7] and nozzle design details are beyond the scope of this paper.

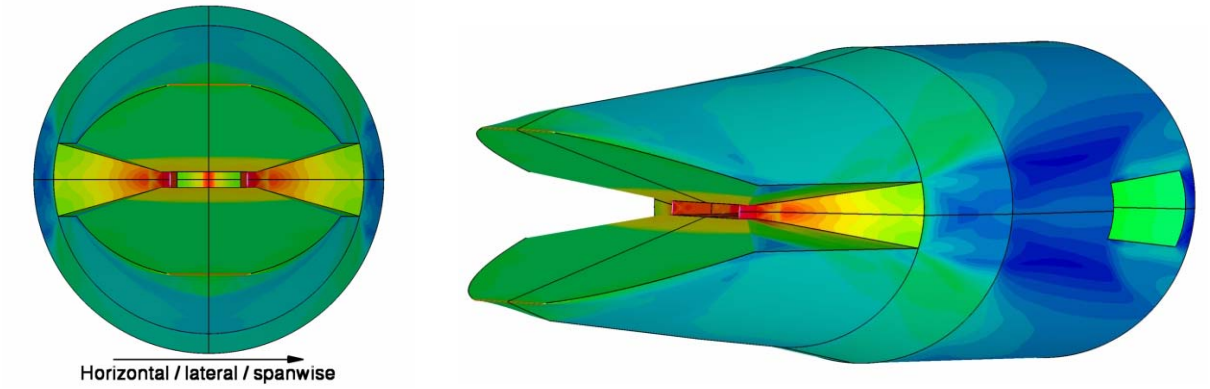

Figure 8. Front and 3D perspective views.

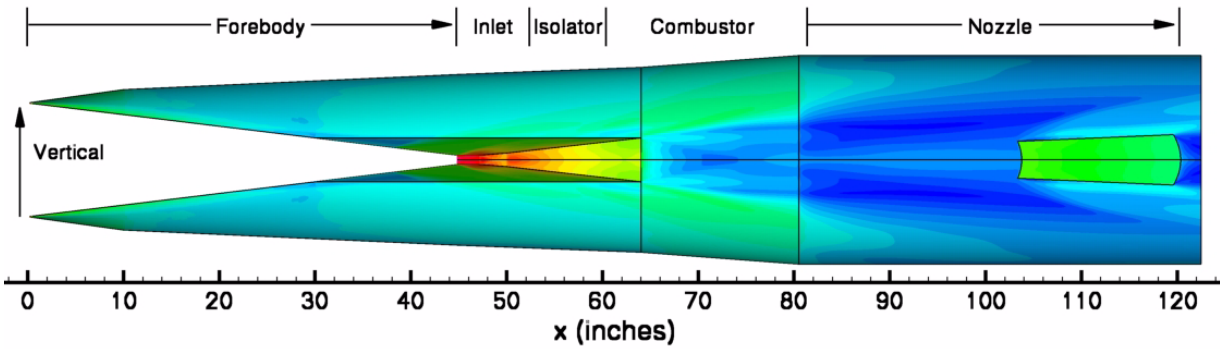

Figure 9. Side view.

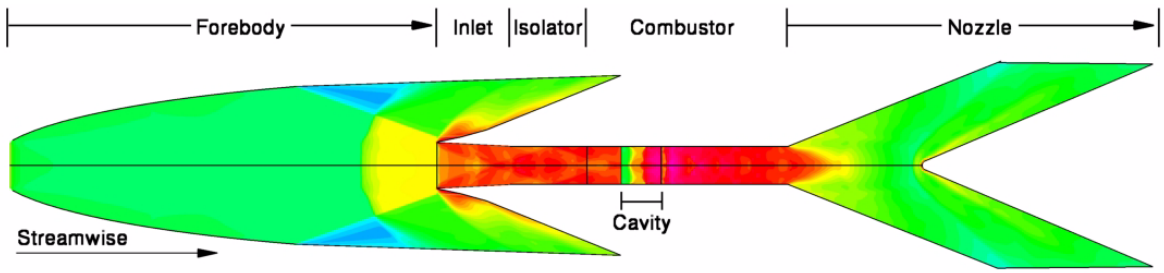

Figure 10. Flowpath surfaces — planform view.

GRID SENSITIVITY STUDY

A grid sensitivity study was completed using the two-dimensional geometry at the centerline before generating a three-dimensional grid. The first consideration was to determine how the flow would be modeled and the required near-wall spacing. The flow from the nose was assumed to be laminar, followed by turbulent flow after the boundary layer trips. The trips were assumed to be fully effective and were modeled computationally by starting the turbulence model 15 inches from the nose. In order to highly resolve the boundary layer a solve-to-the-wall turbulence modeling approach was chosen over a wall matching function approach. Therefore, a small uniform spacing was used for the entire flowpath. Figure 11 shows the increase in skin friction at the trip location and the corresponding y^+ along the flowpath centerline. A constant near-wall spacing of 0.00005 inches was selected for all remaining grid sensitivity studies.

Another important consideration was to determine the grid point distribution. The structured grids were created with Gridgen[8] which has two available stretching functions if the spacing at each boundary is specified; mono-ratio-quad-spline (MRQS) and hyperbolic tangent (Tanh). A comparison of both functions using the same number of points and the same clustering at each end is shown in the right side of Figure 11. The MRQS function has the benefit of being more evenly distributed outside of the boundary layer, while the Tanh function grows more gradually away from the solid boundary; a requirement for laminar and solve-to-the-wall turbulence modeling. The weakness of the Tanh function is that the interior cells can become much larger than the spacing imposed at each end as the solution domain size increases. The solution for creating a high quality grid was to change from the Tanh function to the MRQS function near the edge of the boundary layer. Iteration was necessary since a representative flow solution was required before making the final grid.

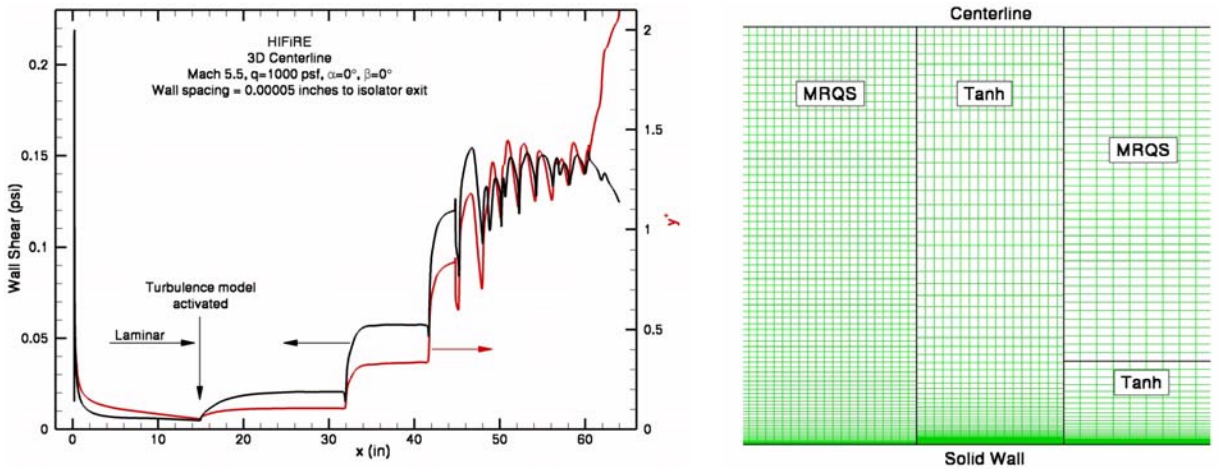

Figure 11. Expected model behavior and comparison of grid stretching functions.

The final step in the grid sensitivity study was determining the required number of points in each direction, or alternatively, a nominal cell size. Despite the relatively simple flowpath geometry, several challenges were encountered. The first challenge was the changing scale of the computational domain. Modeling the forebody flow and inlet flow with the same number of points normal to the wall would lead to either too few points in the forebody region or too many points in the inlet, due to the change in height. In order to model each region with approximately equal resolution, the number of vertical points was changed with a patched computational boundary (not point-to-point matching) ahead of the inlet entrance. The second challenge was the desire to change grid resolution due to fluid dynamic features. This occurred at the end of the forebody where small lateral gradients did not require a small grid spacing compared to the inlet where higher resolution was required to capture the bow shock from the inlet sidewall leading edge. Therefore, a patched computational boundary was used at the inlet entrance plane to increase the number of lateral grid points. The final challenge was limiting the total grid size. Due to the symmetry of the design, cases at 0° α and 0° β could be solved on just one quarter of the full geometry. However, cases at

α or β doubled the grid size and cases at combined α and β would increase the grid size four-fold. The same grid resolution was required for the α and β cases since operability issues may arise under these conditions.

Wall shear was the selected grid convergence criteria because boundary layer separations caused by shock/boundary layer interactions were the primary forebody/inlet operability concern. Wall shear sensitivities due to normal grid variations are shown on the left side of Figure 12. The red line represents the highest resolution solution, while the black and green lines are results with fewer points outside and inside the boundary layer respectively. The inset expands the results at the first shock reflection. The difference between the red and black lines indicates that the bow shock from the nose must be fairly well resolved prior to interacting with the boundary layer, and that 33 points outside the boundary layer was not sufficient. The comparatively small difference between the red and green lines indicates that 33 points through the boundary layer was sufficient. The brown line represents a turbulence model variation resulting in less viscosity and a small separation at the first shock reflection. It also indicates that sensitivity to turbulence modeling is considerably greater than the grid sensitivity. The blue line is the centerline from the final three-dimensional grid with a variable number of points normal to the surface, a consistent 41 points in the boundary layer, and 50 cells per inch in the streamwise direction. A comparison of results for variations in streamwise cell size is shown on the right side of Figure 12. The inset expands the results at the end of the forebody. The black line is the highest resolution and the red and green lines indicate that the calculation is less likely to predict flow separation as the axial cell size increases. The blue line represents the final three-dimensional grid at the centerline. The nominal streamwise cell size determined from the 2D grid sensitivity study (0.02 inches) was used to define the lateral cell size for the 3D grid.

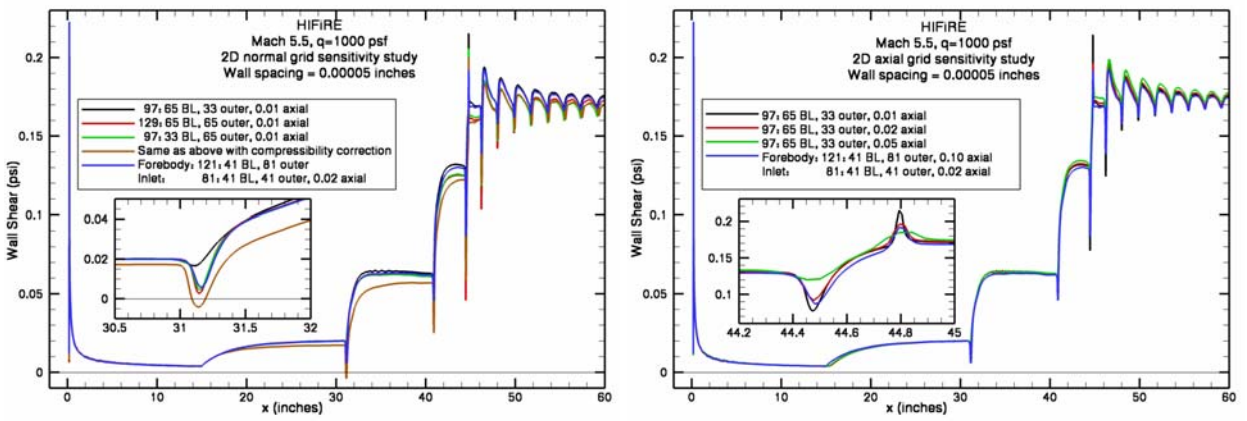

Figure 12. Wall normal and axial grid sensitivity results.

CFD ANALYSIS

COMPUTATIONAL APPROACH

The VULCAN 6.0.1[9] code was used to calculate the flow around the forebody and through the inlet. Symmetry planes were used to model 1/4 of the full geometry for the 0° α and 0° β cases and required 43 million cells. Solutions at angle of attack or sideslip required 86 million cells and one solution performed at a combined angle of attack and sideslip condition required 172 million cells. In order to keep grid and solution files small enough, the problem was divided into multiple segments in the streamwise direction. The grid for each segment was subdivided into multiple blocks for processing on a distributed memory computer cluster. The air flow was modeled as thermally perfect and solved using a low dissipation flux split scheme, full viscous fluxes in each direction, MUSCL extrapolation parameter of 1/3, and a smooth flux limiter. An elliptic solution approach was used for each segment in order to capture boundary layer separation. The first 15 inches of the forebody were solved laminar after which point a solve-to-the-wall k-omega turbulence model was activated.

VERIFICATION OF LOW MACH NUMBER REQUIREMENTS

CFD was used to evaluate inlet operability but not predict the complicated inlet starting process. This was accomplished by initializing the solution domain with freestream conditions (started – supersonic flow throughout) and then inspecting the results of the converged solution. The development of separated flow regions is the primary fluid dynamic phenomenon which could adversely affect the inlet's operation and flow quality provided to the isolator. The lack of large separated regions also increases confidence in the CFD modeling and in the application of engineering tools (i.e. isolator models). Therefore, CFD solutions were performed over a range of conditions to investigate the existence and extent of any separated flow regions. The operability cases were focused at Mach 5.5; the Mach number at which the inlet would have to start following ejection of the shroud. These cases included an α and β variation of 2°. Additional cases at Mach 5 and 4.5 were performed to investigate flow features below the intended starting Mach number. A final case at Mach 4 was performed to verify that the CFD, initialized as started, would predict that the inlet could not remain started. Mach 4 was below the isentropic internal contraction ratio limit and the CFD predicted an inlet unstart as expected.

The present design does not generate oblique shock waves from compression corners, but it does have impinging oblique shock waves which could result in boundary layer separation. The Mach number after the reflection (M_d) compared to the upstream Mach number (M_u) is one measure of the strength of the reflection. Correlations that indicate when shock/boundary layer separation may occur are:[10]

$$\text{Laminar: } M_d < 0.898\, M_u \qquad \text{Turbulent: } M_d < 0.762\, M_u$$

The shock wave pattern generated at the forebody centerline is shown in Figure 13. Boundary layer trips at 15 inches were assumed to create a turbulent boundary layer before the first shock reflection at 32 inches. The Mach number ratios for the first and second shock reflections are both 0.80, therefore according to the above criteria the boundary layer should not separate and the CFD did not predict any separation. The 2° angle of attack shock pattern, at the limit of the design space, is shown in Figure 14. The resulting flow asymmetry is not significant, but the stronger shock generated by the windward side of the forebody (top) creates a stronger first shock reflection on the bottom side. The Mach number ratio of the first shock reflection on the bottom wall is 0.73, which is below the separation correlation criteria. The CFD calculation predicted that the boundary layer was on the verge of separating (wall shear almost zero, but no upstream flow). Therefore, the 7° forebody design was successful in terms of the forebody shock strength and lack of boundary layer separation at the centerline.

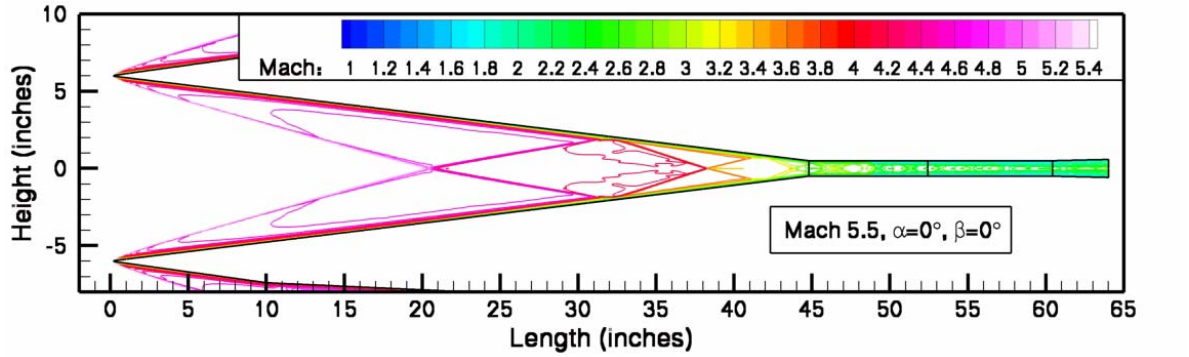

Figure 13. Mach 5.5, α=0° forebody and inlet shock pattern at the centerline.

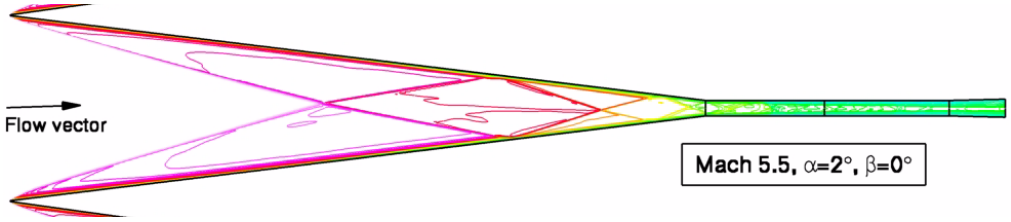

Figure 14. Mach 5.5, α=2° forebody and inlet shock pattern at the centerline.

Of greater concern were the combined forebody shock / inlet sidewall shock / 3D boundary layer interactions in the inlet. In particular, the glancing aspect of the sidewall shock can produce a complex flow and reduce the maximum allowable adverse pressure gradient before separation occurs. Surface wall shear and streamline results for the Mach 5.5 cases are shown in Figure 15. Each image includes the end of the forebody, inlet (up to the vertical line on the sidewall), isolator, and combustor entrance section. The inlet external sidewall and chine surfaces are not shown. The left two images include half of the sidewall height, and one sidewall has been removed from the top right image. Visualizing wall shear was selected so that any separated regions (negative streamwise shear) would be readily apparent. No large scale separated regions develop at any flight condition. However, the top right image shows that a small separation near the inlet sidewall leading edge is possible under certain circumstances, as indicated by the small unshaded region just inside the right sidewall. The separation was caused by a combination of the forebody and inlet sidewall leading edge shocks. It could occur at a variety of flight Mach number and angle of attack combinations which place a forebody shock reflection slightly inside of the inlet. This was a very localized phenomenon and judged not to be a significant operability risk.

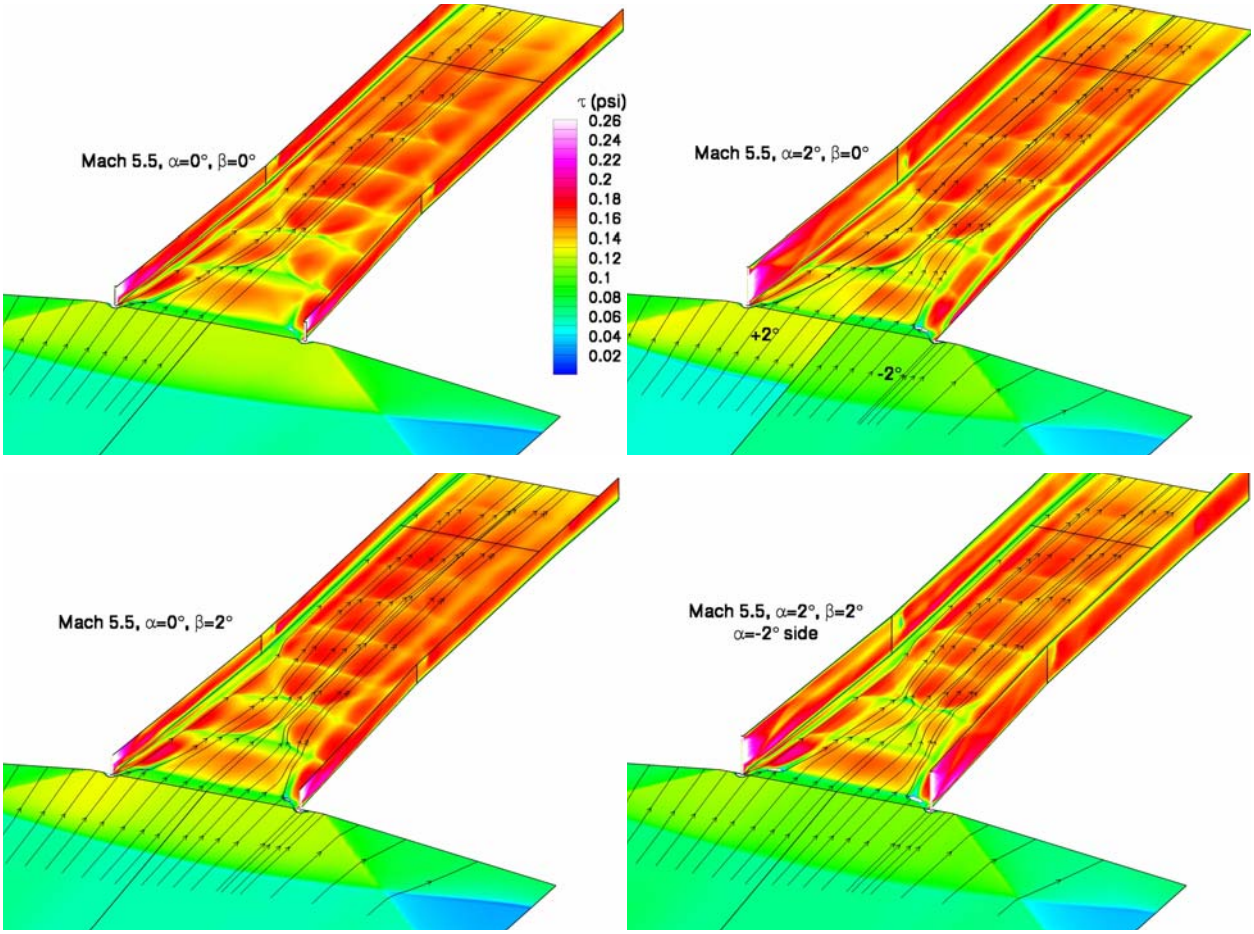

Figure 15. Mach 5.5 wall shear sensitivity to angle of attack and sideslip.

Crossflow contour plots of Mach number were used to assess flow quality in terms of boundary layer behavior and existence of localized low momentum regions which could compromise isolator back pressure capability. Crossflow plots just inside the inlet sidewalls are shown in Figure 16. Low Mach number flow resulting from the sidewall leading edge bluntness are visible near each sidewall. The results indicate that the forebody produced very laterally uniform flow under a variety of flight conditions. Asymmetries from operating at 2° α or β are relatively minor. Figure 17 shows Mach number contours at the isolator entrance and exit, respectively. The boundary layers are fairly uniform around the perimeter without significant undesirable corner effects. Results at Mach 5 and 4.5 reveal well behaved boundary layer flow well below the intended inlet starting Mach number.

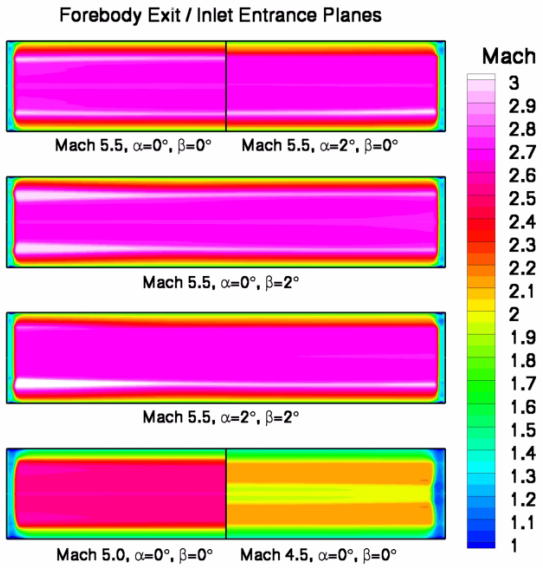

Figure 16. Mach number contours at the inlet entrance.

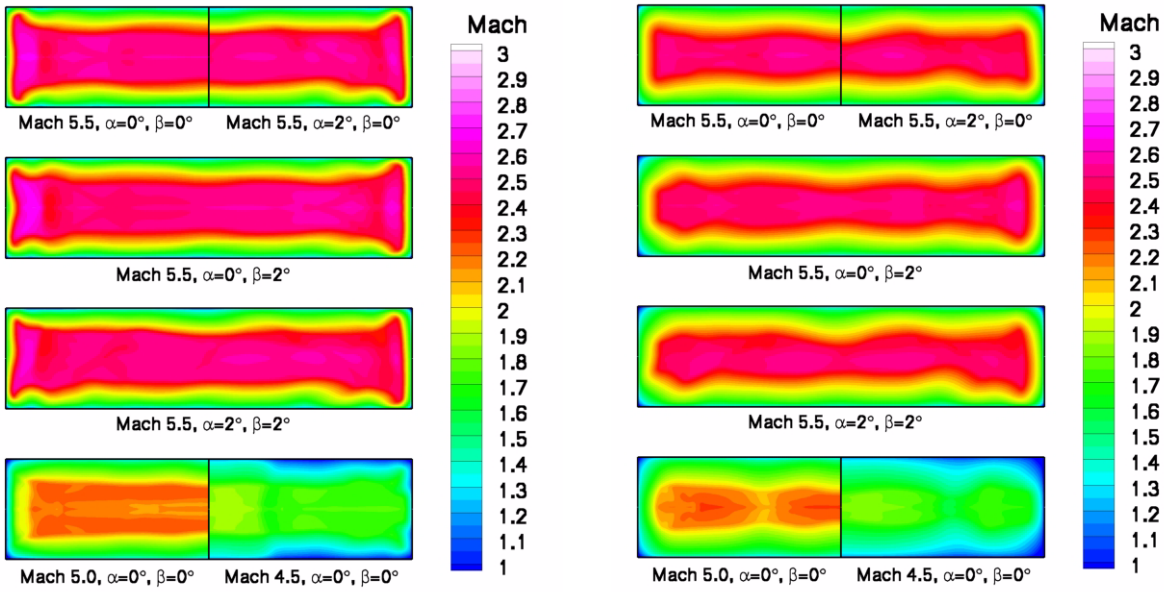

Figure 17. Flow Mach number contours at the isolator entrance (left) and exit (right).

INLET EXIT FLOW SENSITIVITY TO BOOSTER ATTITUDE

Another measure of merit for the compression system was inlet flow sensitivity to booster attitude. While engine mass capture sensitivity to angle of attack is desirable for most hypersonic airbreathing vehicles, in this scramjet engine flight test scenario (α not controlled) minimizing this sensitivity will help maintain the desired fuel equivalence ratio schedule, contribute to stable combustor operation, and simplify post-flight engine performance analysis. Table 1 provides flow property information for the Mach 5.5 operability cases. Spillage was calculated with reference to a 12 by 4.8 inch capture box (no lateral spillage) with freestream flow conditions. The flux conservative approach in the Massflow3d program[11] was used to calculate the one-dimensional flow properties. The spillage, mass capture, and resulting flow properties are almost completely insensitive to α and β variations, within the $\pm 2°$ design space.

Table 1. Inlet exit flow properties for Mach 5.5 operability cases.

Flight Mach #	q (psf)	α (°)	β (°)	Spillage (%)	Capture (lbm/s)	Pres (psi)	Temp (R)	Mach Number	η_{KE} adiabatic
5.5	1000	0	0	27.9	3.44	15.5	1342	2.25	0.9654
		2	0	28.2	3.43	15.7	1357	2.22	0.9635
		0	2	27.7	3.45	15.5	1341	2.25	0.9656
		2	2	27.9	3.44	15.7	1356	2.22	0.9638

NOMINAL FLIGHT TRAJECTORY CASES

Three calculations were performed across a nominal flight trajectory at 0° angle of attack and sideslip. The flight conditions were: Mach=6, q=1817 psf; Mach=7, q=1730 psf; and Mach=8, q=1600 psf. The objectives were to investigate flow features across the Mach range, particularly boundary layer behavior at shock reflection locations, and provide high-resolution computational inflow conditions for combustor calculations. Surface pressure results from the end of the forebody to the combustor entrance are shown in Figure 18. All solutions were performed without any fuel injection or back pressure from combustion. Mach 5, q=2000 psf results are included for completeness and direct comparison. The nose leading edge bow shocks reflect from the opposite forebody surface and propagate through the inlet and isolator creating jumps in pressure on the wide inlet and isolator surfaces in the streamwise direction. The strength of this wave is reduced at Mach 8 when it reflects near the expansion corner at the end of the forebody. The bow shock from the inlet sidewall leading edge propagates laterally across the inlet and isolator and reflects from the opposite sidewall. The resulting "X" pattern becomes shallower as the Mach number increases. Surface streamlines show the effect of the inlet sidewall leading edge, but no significant flow separation was observed at any flight Mach number.

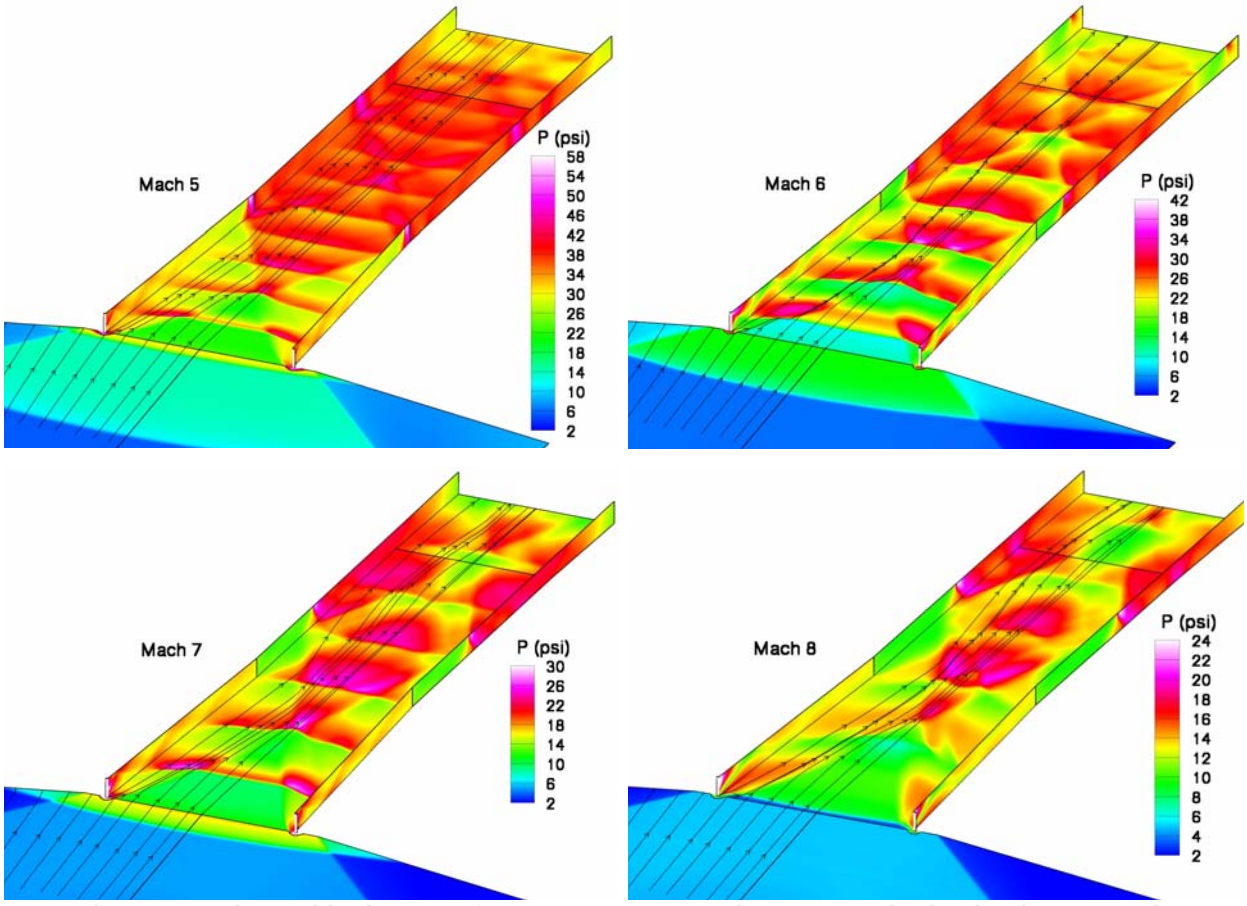

Figure 18. Inlet and isolator surface pressure at Mach 5, 6, 7, and 8 (no back pressure).

Mach number contour plots were used to assess flow quality and boundary layer behavior. Planes at the isolator entrance and a short distance beyond the isolator exit at the beginning of the combustor cavity are shown in Figure 19. The results at the isolator entrance indicate a good core flow without significant boundary layer roll-up or corner effects. The results at the combustor cavity station will be significantly affected by fuel injection, however, these fuel-off solutions reveal a core Mach number roughly half of the flight Mach number. The crossing forebody and inlet sidewall leading edge shocks have not affected the boundary layer too adversely, although they are not laterally uniform. In order to improve the color contrast the lowest contour level is Mach 1.5, which demonstrates that subsonic flow regions are quite small, even in the corners.

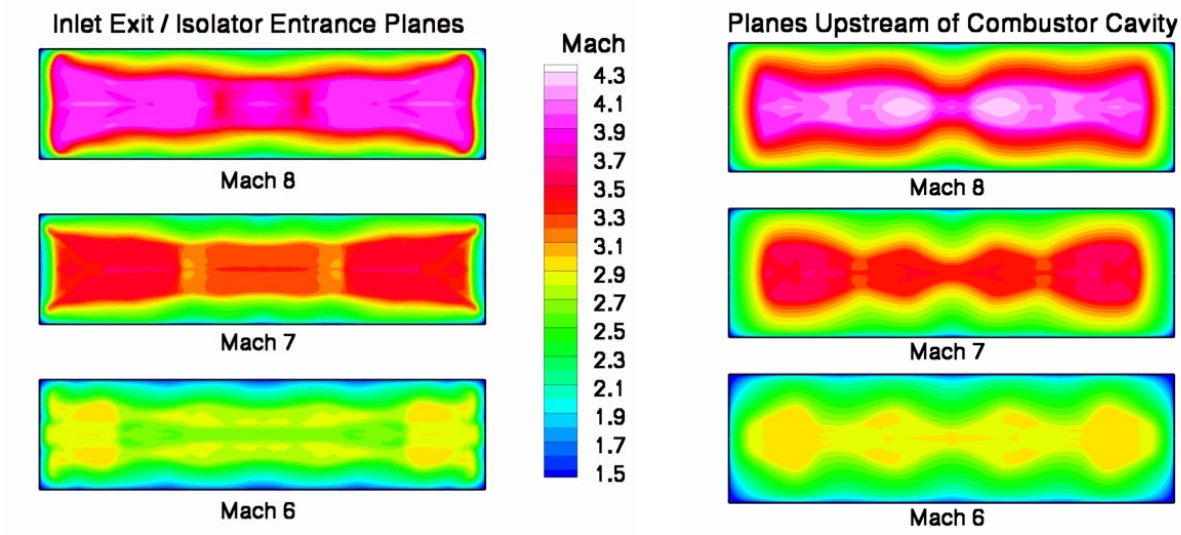

Figure 19. Mach number contours for nominal flight trajectory cases.

Although there was no compression efficiency target, reasonable flow conditions were produced at the isolator entrance at every flight condition analyzed. The mass capture, one-dimensional flow properties and adiabatic kinetic energy efficiency have been tabulated in Table 2. The results show that the spillage decreases as the Mach number increases, which is desirable and expected. The flux conservative one-dimensional inlet exit Mach number is approximately 40% of the flight Mach number. The adiabatic kinetic energy efficiency does not change greatly across the trajectory. Computational planes were extracted at a streamwise location of 48.61 inches in order to provide an inflow boundary condition for flight combustor calculations. This location is approximately half-way through the inlet. A location upstream of the isolator entrance was desired so that the full back pressure capability of the isolator could be modeled, if necessary.

Table 2. Properties for nominal trajectory cases.

Flight Mach Number	q (psf)	α (°)	β (°)	Spillage (%)	Mass Capture (lbm/s)	Inlet Exit Properties			
						Pres (psi)	Temp (R)	Mach Number	η_{KE} adiabatic
5	2000	0	0	30.6	7.38	36.4	1260	1.98	0.9677
6	1817			25.3	5.96	24.4	1380	2.51	0.9644
7	1730			21.9	5.06	18.1	1490	2.99	0.9652
8	1600			19.4	4.21	13.8	1620	3.42	0.9659

HIGH DYNAMIC PRESSURE HEAT LOAD CASES

Six cases were completed to provide heat load information for thermal analysis. Two constant wall temperature solutions were performed at three Mach numbers: 5, 6, and 8. The wall temperatures were 540 and 1080 R at Mach 5, 1080 and 1440 R at Mach 6, and 1440 and 1800 R at Mach 8. The load set allows thermal analysts to determine the heat flux to the structure as different sections of the surface heat up at different rates through the trajectory after shroud deployment. For these cases the computational grid was extended to include the combustor, nozzle, and external flow to beyond the nozzle exhaust opening. The grid included 75.5 million cells to model one-quarter of the geometry, taking advantage of vertical and lateral symmetry. Results for the external surfaces are shown in the left image of Figure 20. The flow was modeled as turbulent after 15 inches on the flowpath surfaces and after 30 inches on the external surfaces. Heat flux levels were generally low except at the forebody and inlet sidewall leading edges. The computational exit boundary shows Mach contours. The right side of Figure 20 shows internal results with the top half of the vehicle removed. The heat flux to the combustor and nozzle changes with fuel injection and combustion, but fuel-off solutions were performed to provide an initial load set.

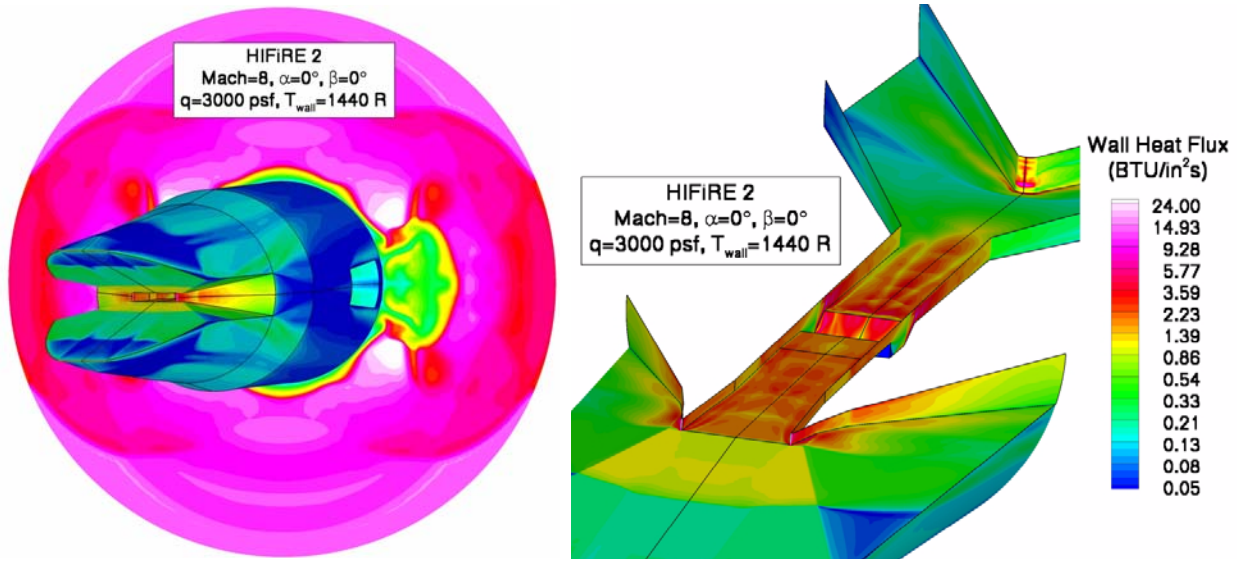

Figure 20. External and internal surface heat flux contours at Mach 8, no fuel (note log scale).

Heat flux levels along the flowpath and sidewall surfaces were extracted for comparison. Of particular concern were the forebody and inlet sidewall blunt leading edges. Each has a radius of 0.030 inches which results in high stagnation point heat flux. The total heat load may not be very high because the affected area is so small. However, the small size also limits the thermal capacity and conductive ability of the part. Thermal analysis will have to verify the survivability of the final design and selected material. Results for the centerline of the main flowpath surface are plotted in Figure 21. The left image is an expanded region near the vehicle nose. Results from the StagHeat[12] code are included for comparison. This code uses the Fay and Riddell correlation and modeled the gas in chemical equilibrium. CFD results are plotted around the radius. The maximum difference between the two solution methodologies is 8.4%. The right image shows that the heat flux to the inlet and isolator is between 0.7 and 2 BTU/in^{2}s. The heat flux generally drops through the expanding combustor except at Mach 8 where a strong shock at the end of the cavity increases the flow static temperature significantly. However, those results will change significantly with fuel injection and combustion. The spike at the end of the plot is a recirculation region which develops ahead of the nozzle centerbody. Results for the centerline of the engine sidewall are shown in Figure 22. The left image shows an expanded region at the inlet sidewall leading edge. The CFD and StagHeat results have a maximum difference of 8.8%, with a peak heat flux nearing 25 BTU/in^{2}s. The remainder of the inlet and isolator sidewall experiences levels similar to the flowpath centerline. The color contour inset shows the primary area of concern at the inlet sidewall leading edge at Mach 8 with a 1440 R wall temperature. Table 3 reveals that the thicker boundary layers created by higher surface temperatures produced greater compression, but that mass capture was not significantly affected.

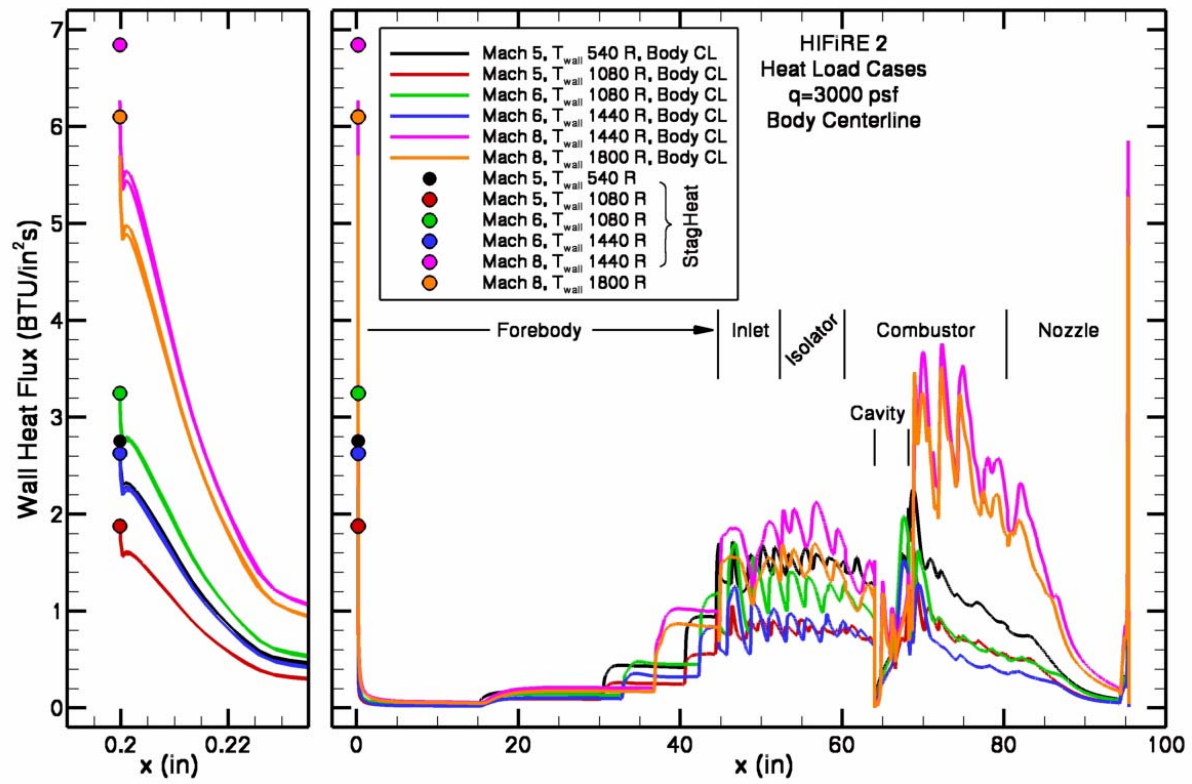

Figure 21. Flowpath centerline heat flux (no fuel injection).

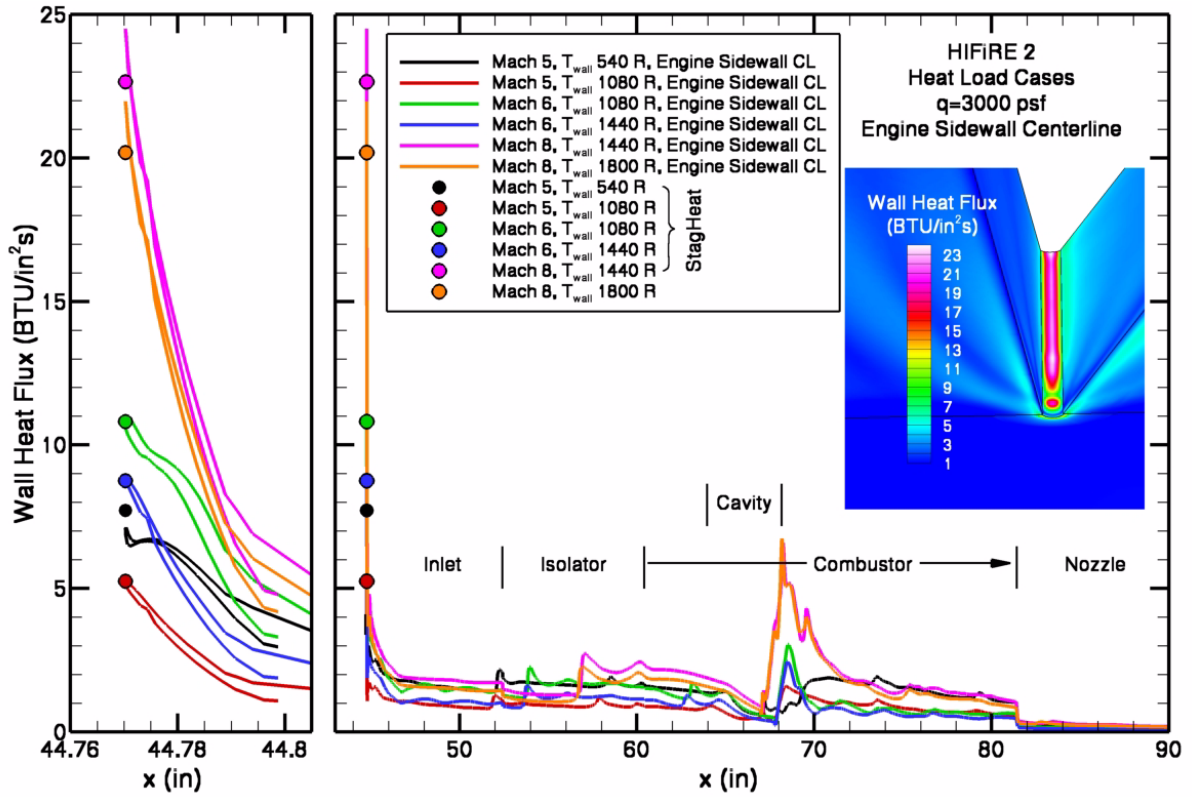

Figure 22. Engine sidewall centerline heat flux (no fuel injection).

Table 3. Properties for heat load cases.

Flight Mach Number	q (psf)	Wall Temp (R)	Spillage (%)	Mass Capture (lbm/s)	Inlet Exit Properties			
					Pres (psi)	Temp (R)	Mach Number	η_{KE} adiabatic
5	3000	540	30.8	11.03	53.0	1260	2.00	0.9675
		1080	30.8	11.03	56.3	1300	1.95	0.9611
6		1080	26.3	9.80	40.5	1390	2.50	0.9605
		1440	26.4	9.79	41.4	1420	2.46	0.9577
8		1440	19.9	7.92	25.7	1610	3.43	0.9644
		1800	20.0	7.91	26.1	1630	3.41	0.9630

SUMMARY

The HIFiRE 2 flight test will investigate ramjet-scramjet mode transition and Mach 8+ scramjet performance of a hydrocarbon fueled combustor design in flight. The experiment technique will use a spin-stabilized booster rocket and a suppressed trajectory. The combustor test window was defined as an accelerating trajectory from Mach 5.5 to Mach 8.5, nominally at a constant dynamic pressure between 1000 and 3000 psf. There were three requirements for the compression system. First, it had to start prior to Mach 5.5. While time accurate analysis of the starting process was not performed, fairly high confidence was achieved by selecting an internal contraction ratio which meets the Kantrowitz inlet starting criteria for flight at Mach 4.5. Second, minimal boundary layer separation had to be predicted at Mach 5.5 over an angle of attack and sideslip range of 2°. Finally, a minimum combustor entrance pressure of 1/2 atmosphere was required at Mach 8.5, q=1000 psf. CFD was used to verify that these requirements were achieved.

A number of constraints and selected approaches also affected the design process and final forebody and inlet design. The maximum physical size was limited to fit within a 22 inch outer diameter shroud. A fixed geometry design solution was found. Two-dimensional design concepts were used to facilitate the use of shock boundary layer separation correlations and to increase modeling confidence by maintaining well behaved boundary layer flow. The forebody compression angle was constrained to 7° and boundary layer trips specified in order to meet the minimal boundary layer separation requirement. A radius of 0.030 inches was selected for all leading edges and should not require active cooling. The forebody and inlet sidewall included angles were set at 15° which should not require an elaborate structural design. The inlet sidewalls were limited to 3° of compression in order to limit the strength of the bow shock crossing the forebody boundary layer. Chine surfaces were added to the end of the forebody to more easily spill the flow not captured by the inlet and facilitate inlet starting.

Additional solutions were performed through the nominal flight trajectory and at multiple surface temperatures. The trajectory cases allowed the inlet performance and flow features to be assessed at Mach 6, 7, and 8. A computational plane at the middle of the inlet was extracted as an inflow plane for on-going computational combustor analysis. Heat transfer results from solutions performed at high dynamic pressure and multiple wall temperatures enable transient thermal analysis of the structure.

A planar, fixed geometry, mixed compression forebody and inlet concept was designed and shown to provide high quality flow to the isolator throughout the flight trajectory and over a range of booster attitudes. “High quality” emphasizes the lack of separated regions, streamwise vortices, significant corner effects, or other local phenomenon which would compromise isolator back pressure capability. The design exceeded program requirements. While the present design was not a predecessor to any free-flying vehicle, other boosted scramjet combustor flight experiments may benefit from the simplicity and effectiveness of this design concept.

REFERENCES

1). Jackson, K. and Hass, N., "HIFiRE Flight 2 Scramjet Flight Experiment", 55th JANNAF Propulsion Meeting, Boston, MA, May 2008.

2). Smart, M., Hass, N., and Paull, A., "Flight Data Analysis of the HyShot 2 Scramjet Flight Experiment", AIAA Journal, Vol. 44, No. 10, 2006, pp. 2366-2375.

3). Pellet, G., Vaden, S., and Wilson, L., "Gaseous Surrogate Hydrocarbons for a HIFiRE Scramjet that Mimic Opposed Jet Extinction Limits for Cracked JP Fuels", 55th JANNAF Propulsion Meeting, Boston, MA, May 2008.

4). Kantrowitz, A., and Donaldson, C., "Preliminary Investigation of Supersonic Diffuser", NACA WRL-713, 1945.

5). Glass, D., "Hyper-X Mach 10 Leading-Edge Evaluation", JANNAF Propulsion Meeting, Monterey, CA, November, 2000.

6). Berry, S., Daryabeigi, K., Wurster, K., and Bittner, R., "Boundary Layer Transition on X-43A", 38th AIAA Fluid Dynamics Conference, June 23-26, 2008.

7). Gruber, M., Jackson, K., Jackson, T., and Liu, J., "Hydrocarbon-Fueled Scramjet Combustor Flowpath Development for Mach 6 – 8 HIFiRE Flight Experiments", 55th JANNAF Propulsion Meeting, Boston, MA, May 2008.

8). Gridgen version 15.10, Pointwise®, Inc.

9). VULCAN, http://vulcan-cfd.larc.nasa.gov/index.html.

10). Heiser, W. and Pratt, D., "Hypersonic Airbreathing Propulsion", AIAA Education Series, 1994.

11). Meyer, B., "User Manual and Methodology for One-Dimensionalization Code: Massflow3d version 8.4", Technical Note 06-474, NASA Langley Contract NAS1-00135B, May 11, 2006.

12). Vince Cuda, Jr., "Leading Edge Thermal Loads for Hypersonic Vehicle Design Using the StagHeat Code", Technical Note 05-467, NASA Langley Contract NAS1-00135B, November 11, 2005.

NOMENCLATURE

α = angle of attack
β = angle of sideslip
η_{KE} = kinetic energy efficiency
CFD = computational fluid dynamics
q = dynamic pressure
2D = two-dimensional
3D = three-dimensional